Numerical Heat Transfer, Part A: Applications
An International Journal of Computation and Methodology

ISSN: 1040-7782 (Print) 1521-0634 (Online) Journal homepage: www.tandfonline.com/journals/unht20

Analysis of two-equation RANS turbulence models for accurate numerical analysis of vortex tubes

O. A. A. Awan, R. Sager, E. Juntasaro & M. Wirsum

To cite this article: O. A. A. Awan, R. Sager, E. Juntasaro & M. Wirsum (2026) Analysis of two-equation RANS turbulence models for accurate numerical analysis of vortex tubes, Numerical Heat Transfer, Part A: Applications, 87:1, 2534396, DOI: 10.1080/10407782.2025.2534396

To link to this article: https://doi.org/10.1080/10407782.2025.2534396

NUMERICAL HEAT TRANSFER, PART A: APPLICATIONS
2026, VOL. 87, NO. 1, 2534396
https://doi.org/10.1080/10407782.2025.2534396

Analysis of two-equation RANS turbulence models for accurate numerical analysis of vortex tubes

O. A. A. Awan[a,b], R. Sager[b], E. Juntasaro[a], and M. Wirsum[b]

[a]The Sirindhorn International Thai-German Graduate School of Engineering (TGGS), King Mongkut's University of Technology North Bangkok, Thailand; [b]Institute of Power Plant Technology, Steam and Gas Turbines, RWTH Aachen University, Germany

ABSTRACT

Increasing the efficiency of existing and new energy systems is necessary to accelerate the shift toward sustainability. One promising avenue for achieving this objective is to integrate new devices into the existing energy systems, such as vortex tubes. However, the incorporation of vortex tubes into the energy systems is restricted due to their limited development and inadequate efficiency. Therefore, there is growing demand on overcoming the drawbacks of vortex tubes. Therefore, a lot of research is being done to overcome these drawbacks. Computational research is more favored over experimental research to exploit the advantages of time and cost efficiency. However, there is still no concrete answer to the question: What is the most appropriate two-equation RANS turbulence model for accurate numerical analysis of vortex tubes? Different authors gave different recommendations in the past, making this question more ambiguous. Therefore, this research aims to address this challenge. In this regard, two different geometric models are considered. A mesh-independence study and a y^+ study have been conducted to obtain an appropriate mesh. For the first geometry, the SST k-ω model has been selected for the mesh-independence and y^+ studies, while the standard k-ϵ model has been used for the other geometric model. Afterward, a turbulence model study is conducted for both geometric models by considering two-equation RANS turbulence models. The performance of different turbulence models is evaluated with various reference data. For both geometric models, the standard k-ϵ turbulence model outperforms other considered turbulence models when compared with the experimental data. This is also in line with the outcomes of most studies in the past. These results could be used to further investigate the performance of vortex tubes under different geometric and operating parameters.

ARTICLE HISTORY
Received 5 September 2024
Revised 26 October 2024
Accepted 30 May 2025

KEYWORDS
Energy efficiency; k-ϵ turbulence model; Ranque-Hilsch vortex tube (RHVT); RANS CFD; turbulence modeling

1. Introduction

Since the industrial revolution in the late nineteenth century, energy conversion has relied mainly on fossil fuels, resulting in CO_2 and other greenhouse gas emissions that contribute to global warming. To address the climate crisis, energy conversion and use must become more sustainable and environmentally friendly. There are two primary ways to make energy conversion and

CONTACT O. A. A. Awan osamaaliahmadawan@outlook.com The Sirindhorn International Thai-German Graduate School of Engineering (TGGS), King Mongkut's University of Technology North Bangkok, Bangkok, Thailand

Nomenclature

Latin symbol	
A	area [mm^2]
d	diameter [mm]
D	RHVT diameter [mm]
L	RHVT length [mm]
$\dot{m}$	mass flow [kg/s]
p	pressure [Pa]
T	temperature [K]
y^+	dimensionless wall distance [–]
F	force [N]
f	external forces per unit volume [N/m^3]
R	gas constant [J/kg K]
Q	heat added to the system [J]
τ	stress tensor [–]
t	time [s]
v	velocity [mm/s]
W	work done by the system [J]
e	energy per unit mass [J/kg]

Greek symbols	
Δ	difference between two values [–]
μ_c	cold mass fraction [–]
∇	gradient operator
ρ	density [kg/m^3]
ν	Eddy viscosity [m^2/s]

Subscripts	
c	cold outlet
cfd	computational fluid dynamics
exp	experiment
h	hot outlet
i	inlet
t	total
VT	vortex tube
CS	control surface
CV	control volume
v	volume

Abbreviations	
3D	three dimensional
COP21	The 21st Conference of the Parties
GWP	global warming potential
k-ϵ	standard k-epsilon
k-ω	standard k-omega
RNG k-ϵ	Re-Normalization Group k-epsilon
RANS	Reynolds-Averaged Navier-Stokes
RSM	Reynolds stress model
SA	Spalart-Allmaras model
RHVT	Ranque-Hilsch vortex tube
SST-SAS	Shear Stress Transport–Scale-Adaptive Simulation
SST k-ω	Shear Stress Transport k-omega
TSE	temperature separation effect

consumption more eco-friendly: replacing fossil fuels with renewable energy for electricity generation and improving the efficiency of new and existing energy systems. One way to increase efficiency and reduce energy waste is to incorporate new devices into energy systems. One such device is the Ranque-Hilsch Vortex Tube (RHVT), a simple thermal device with no moving parts.

The vortex tube was first invented by the French scientist Georges J. Ranque in the early 1930s. However, a more adequate explanation of the temperature separation effect (TSE) inside the RHVT was given by the German physicist Rudolf Hilsch in 1947 [1]. The RHVT divides the compressed incoming fluid stream into two separate streams. Figure 1 shows the working principle of the RHVT. The resulting fluid streams exit the RHVT through both outlets (hot outlet and cold outlet). The fluid stream exiting from the hot outlet has a higher temperature than the incoming stream, while the fluid stream exiting from the cold outlet has a lower temperature than the incoming stream. The RHVT has an inlet section with variable tangential nozzles, supplemented with a vortex generator. The compressed fluid stream enters through the inlet nozzles and is given a swirl by the vortex generator. The flow through the RHVT is controlled by a valve at the hot outlet to regulate μ_c, which is the ratio of the mass flow rate of the fluid stream leaving the cold outlet to the mass flow rate of the incoming stream.

The ability of the RHVT to separate a fluid stream into two streams with different temperatures can be very useful in various applications, such as refrigeration cycles [2,3] and heat pumps [4,5]. However, the RHVT has not received much attention in the past due to its inadequate efficiency and limited development. Therefore, it is currently receiving increasing attention from researchers and industry to exploit its advantages in several energy systems and thus understand the underlying effects.

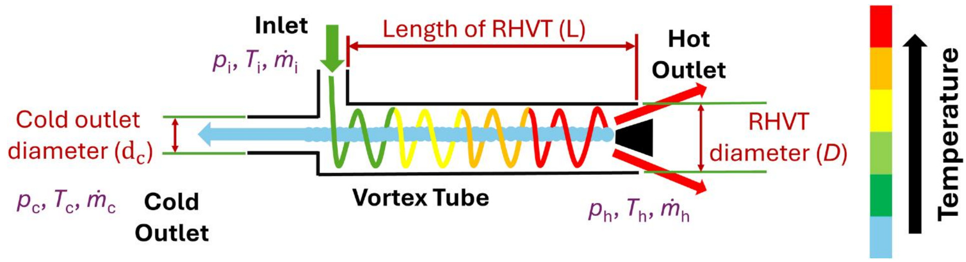

Figure 1. Working principle of the RHVT.

Table 1. Different turbulence models used in recent research studies.

Research article	k-ϵ	k-ω	SST k-ω	SAS SST	SA	RNG k-ϵ	RSM	Realizable k-ϵ	ASM	Best turbulence model
Bagdad *et al.* [6]	✓	✓	✓	×	×	×	✓	×	×	RSM
Bazgir *et al.* [10]	✓	×	✓	×	×	✓	×	✓	×	RNG k-ϵ
Chýlek *et al.* [11]	✓	✓	✓	×	×	×	✓	✓	×	k-ϵ
Singh *et al.* [17]	✓	×	✓	×	×	×	×	×	×	k-ϵ
Dyck *et al.* [18]	✓	✓	✓	✓	×	×	×	×	×	SAS SST
Lagardeux *et al.* [19]	✓	×	✓	×	×	×	×	×	×	SST k-ω
Sadeghiseraji *et al.* [20]	✓	×	✓	×	×	×	×	×	×	k-ϵ
Hu *et al.* [21]	✓	×	✓	×	✓	×	×	✓	×	Realizable k-ϵ
Thakare and Parekh [22]	✓	✓	×	×	✓	×	×	×	×	k-ϵ
Liu and Liu [23]	✓	×	✓	×	×	✓	✓	✓	×	Realizable k-ϵ
Eiamsa-ard and Promvonge [24]	✓	×	×	×	×	×	×	×	✓	ASM

There are three main types of research investigation approaches: experimental, computational, and analytical. Among these, the computational approach has received substantial attention in the recent past due to its advantages of cost and time efficiency, flexibility, reproducibility, and adaptability compared to other approaches. Therefore, researchers have put considerable efforts into conducting accurate computational analysis of the flow phenomena inside the RHVT. Although substantial efforts have been invested in the accurate analysis of the RHVTs, certain questions remain unresolved.

One of these questions is: What is the best modeling approach for the highly turbulent flow phenomena inside the RHVT to accurately predict and analyze its behavior? As there are many approaches available, such as two-equation Reynolds-averaged Navier–Stokes equations (RANS) turbulence model, LES, DNS, and RSM. It is difficult to conclude which approach is more feasible for numerical analysis of the RHVT. RSM has received a lot of attention in recent years. On the one hand, several authors have concluded that RSM is the most appropriate turbulence model for the numerical analysis of flow phenomena inside the RHVT [6–9]. On the other hand, RSM is associated with increased computational cost and convergence difficulty [10–14]. Furthermore, although LES and DNS are the most accurate techniques, they considerably increase the computational cost [9,15,16]. Therefore, most research on RHVTs employs two-equation RANS turbulence models. Additionally, since RHVTs have not received much attention in the past due to their drawbacks, using two-equation turbulence models offers the advantage of rapid research to better understand the TSE inside RHVTs. However, another question remains: Which two-equation RANS turbulence model is best for accurate analysis of RHVTs? To date, there is no concrete outcome regarding which two-equation RANS turbulence model is the most suitable for accurate analysis of RHVTs. As a result, different turbulence models have been used by different authors to determine the most appropriate one. Table 1 shows the different turbulence models investigated by various authors and their recommended turbulence model.

Given the previously available work, one may question why an additional study on this topic is necessary. The reasons for this are as follows:

1. Some previous studies were carried out in 2D [19,22,24]. However, advances in computational resources now allow for more detailed 3D analysis, which may lead to more accurate results [9,25].
2. The near-wall treatment is crucial for reliable numerical results. However, some previous studies lacked detailed information on this aspect, which may call the credibility of their results into question [6,10,23].
3. Although some prior studies mainly focused on the effect of geometric and operational parameters on RHVT performance, they recommended specific turbulence models based on limited comparative analysis [10,17].
4. Some previous studies used structured meshes [20]. However, given the complex geometry of the RHVT, unstructured meshes could provide a more accurate flow field analysis.
5. Recommendations on this question by various authors are conflicting, which has complicated the topic further.

Therefore, the primary objective of this work is to determine which two-equation turbulence model predicts the most accurate TSE when compared with reference data. This is accomplished through numerical simulations of two different 3D models of the RHVT. The results are then compared with the respective reference data, and the outcomes are discussed. The details of this research study unfold across the following sections of this article: Section 2 outlines the theoretical background. Section 3 discusses the development of numerical model, Section 4 presents the research results, and the last section summarizes the conclusions and outlines the future objectives of this research.

2. Governing equations

To accurately predict the flow field and temperature of the fluid inside the RHVT, the fluid domain needs to be divided into infinitesimally small control volumes. The fundamental conservation equations need to be solved for each of the control volumes simultaneously. These equations adhere to three primary conservation laws: mass, momentum, and energy (see Eqs. 1–3) [26].

$$\frac{d}{dt}\left(\int_{CV}\rho dV\right)+\int_{CS}\rho(\mathbf{v}\cdot\mathbf{n})dA=0 \tag{1}$$

$$\sum\vec{F}=\frac{d}{dt}\left(\int_{CV}\rho\mathbf{v}\ dV\right)+\int_{CS}\rho\mathbf{v}(\mathbf{v}\cdot\mathbf{n})dA \tag{2}$$

$$\dot{W}_{\text{shaft, net-in}}+\dot{Q}_{\text{net-in}}=\frac{d}{dt}\left(\int_{CV}e\rho\ dV\right)+\int_{CS}\left(\frac{p}{\rho}+e\right)\rho(\mathbf{v}\cdot\mathbf{n})dA \tag{3}$$

where ρ is the fluid density, t is time, CV is the control volume, CS is the control surface, $\mathbf{v}$ is velocity, $\mathbf{n}$ is the unit normal vector, dV and dA are differential volume and area, $\vec{F}$ is force, $\dot{W}_{\text{shaft,net-in}}$ is net shaft work, $\dot{Q}_{\text{net-in}}$ is net heat transfer, e is specific energy, and p is pressure.

These conservation laws form the foundation for understanding the behavior of fluid particles. By using the conservation equations and assuming fluid as a continuum, one can derive Navier-Stokes equations, which provide the most comprehensive explanation of a fluid behavior. They are a set of nonlinear, coupled, and second-order partial differential equations. They can be used to calculate the 3D, unsteady, and viscous flow. The general vector form of the Navier-Stokes equations is given by Eq. (4).

$$\rho \frac{D\mathbf{v}}{Dt} = -\nabla p + \nabla \cdot \boldsymbol{\tau} + f \tag{4}$$

where $\frac{D\mathbf{v}}{Dt}$ is the material derivative of the velocity, ∇p is the pressure gradient, $\nabla \cdot \boldsymbol{\tau}$ is the divergence of the stress tensor, and **f** represents body forces.

The Navier-Stokes equations are not sufficient for a closed solution so that additional closure relations and boundary conditions are required. The equation of state is used to account for compressibility effects. It relates the temperature, pressure, and density of the fluid to close the system of equations for accurate analysis. Equation (5) gives the equation of state for an ideal gas [26].

$$p = \rho RT \tag{5}$$

Furthermore, the Navier-Stokes equations require initial and boundary conditions to specify the starting state and the physical constraints. In addition, turbulence model equations are required for closure due to the complex, chaotic, and 3D nature of turbulent flow. One way is to perform DNS calculations, but they are very complex and require a lot of computing power. Therefore, to reduce the computational cost while still benefiting from DNS, LES can be used. In LES, the large eddies are calculated and the smaller eddies are modeled by different available models. However, LES also requires substantial computational resources. To overcome this, different authors have proposed various modeling equations based on empirical relations from experimental investigations. These models are known as RANS models and can be broadly categorized into eddy viscosity models and second moment closure models. Eddy viscosity models include algebraic models, such as mixing length and Baldwin-Lomax, one-equation models, such as SA, k-model, and two-equation models, such as k-ϵ, k-ω, and SST k-ω models. Meanwhile, second moment closure models include algebraic RSM, differential RSM, and others. Among these, eddy viscosity models are the most widely used. Furthermore, among the eddy viscosity models, two-equation models are generally preferred because they require less computational resources and provide adequate predictions of the flow compared to second-moment closure models. This is because although second-moment closure models provide a more accurate solution, they require significant computational resources. The Navier-Stokes equations (Eq. 7) along with the continuity (Eq. 6) and energy equations (Eq. 8) are solved by two-equation RANS turbulence models.

$$\frac{\partial}{\partial x_i}(\rho U_i) = 0 \tag{6}$$

$$\frac{\partial}{\partial x_{\mathrm{j}}}(\rho U_{\mathrm{i}} U_{\mathrm{j}}) = -\frac{\partial P}{\partial x_i} + \frac{\partial}{\partial x_j}(t_{ij} + \rho \tau_{ij}) \tag{7}$$

where $t_{ij} = 2\mu \overline{S}_{ij}$, $\rho\tau_{ij} = 2\mu_T \overline{S}_{ij} - \frac{2}{3}\rho k \delta_{ij}$, $\overline{S}_{ij} = S_{ij} - \frac{1}{3}\frac{\partial U_k}{\partial x_k}\delta_{ij}$, and $S_{ij} = \frac{1}{2}\left(\frac{\partial U_i}{\partial x_j} + \frac{\partial U_j}{\partial x_i}\right)$.

$$\frac{\partial}{\partial x_j}\left[\rho U_j\left(h + \frac{1}{2}U_i U_i\right)\right] = \frac{\partial}{\partial x_j}\left[U_i(t_{ij} + \rho\tau_{ij}) + \left(\frac{\mu}{Pr_L} + \frac{\mu_T}{Pr_T}\right)\frac{\partial h}{\partial x_j}\right] \tag{8}$$

where h is the enthalpy, Pr_L is the laminar Prandtl number, and Pr_T is the turbulent Prandtl number.

Among the two-equation RANS turbulence models, the k-ϵ turbulence model is the most widely used for the numerical analysis of RHVTs. It was initially proposed by Jones and Launder in 1972, without damping functions but with empirical constants [27]. Equation (9) is the transport equation for k together with the transport equation for ϵ in Eq. (10).

$$\frac{\partial}{\partial x_{\mathrm{j}}}(\rho U_{\mathrm{j}} k) = P_{\mathrm{k}} - \rho\epsilon + \frac{\partial}{\partial x_{\mathrm{j}}}\left[\left(\mu + \frac{\mu_{\mathrm{T}}}{\sigma_k}\right)\frac{\partial k}{\partial x_{\mathrm{j}}}\right] \tag{9}$$

where $P_{\mathrm{k}} = \rho\tau_{ij}\frac{\partial U_{\mathrm{i}}}{\partial x_{\mathrm{j}}}$.

$$\frac{\partial}{\partial x_j}(\rho U_j \epsilon) = C_{\epsilon 1}\frac{\epsilon}{k}P_k - C_{\epsilon 2}\rho\frac{\epsilon^2}{k} + \frac{\partial}{\partial x_j}\left(\mu + \frac{\mu_T}{\sigma_\epsilon}\right)\frac{\partial \epsilon}{\partial x_j} \tag{10}$$

where $C_{\epsilon 1} = 1.44$, $C_{\epsilon 2} = 1.92$, $\sigma_k = 1.0$, $\sigma_\epsilon = 1.3$, and $\mu_t = \rho C_\mu \frac{k^2}{\epsilon}$.

Furthermore, in 1993, Wilcox introduced a model by defining $\epsilon = C_\mu k\omega$, where C_μ is an empirical constant [27]. The transport equations for k and ω of the k-ω turbulence model are given in Eqs. (11) and (12), respectively.

$$\frac{\partial}{\partial x_j}(\rho U_j k) = P_k - C_\mu \rho k\omega + \frac{\partial}{\partial x_j}\left[\left(\mu + \frac{\mu_T}{\sigma_k}\right)\frac{\partial k}{\partial x_j}\right] \tag{11}$$

$$\frac{\partial}{\partial x_j}(\rho U_j \omega) = C_{\omega 1}\frac{\omega}{k}P_k - C_{\omega 2}\rho\omega^2 + \frac{\partial}{\partial x_j}\left(\mu + \frac{\mu_T}{\sigma_\omega}\right)\frac{\partial \omega}{\partial x_j} \tag{12}$$

where $C_{\omega 1} = \frac{5}{9}$, $C_{\omega 2} = \frac{3}{40}$, $C_\mu = 0.09$, $\sigma_\omega = \sigma_k = 2$, and the eddy viscosity is given as $\mu_T = \rho\frac{k}{\omega}$.

The SST k-ω turbulence model is a modified form of the k-ω turbulence model. In 1994, Menter proposed a two-zone formulation to rectify the spurious behavior of the k-ω model under free-stream conditions [27]. This approach uses the k-ω model near the wall and the k-ϵ model for the rest of the flow inside the boundary layer. The transition between these formulations is achieved by a smooth interpolation process. Further details on other turbulence models can be found in Ref. [27].

3. Numerical setup

3.1. Geometry

As mentioned above, this study considers two different 3D RHVT geometric models. Although some previous studies have considered 2D models, their results lack quantitative accuracy [9,25]. Therefore, only 3D models are considered in the present work. The first model resembles the geometry investigated by Rafiee and Sadeghiazad [8]. It has two inlet tangential nozzles. The experimental results from Rafiee and Sadeghiazad [8] are used to validate the current results.

The second model is similar to the commercially available Exair (model 3225) RHVT [28], which is also used by Skye *et al.* [14]. However, Skye *et al.* [14] did not provide information on the geometry of control valve for their experimental study. In another study, Qyyum *et al.* [29] found that a truncated-type hot control valve yielded better results compared to a cone-type hot control valve when compared with the experimental results. The other dimensions of geometric model in study of Qyyum *et al.* [29] are similar to that of experimental study of Skye *et al.* [14]. Therefore, a truncated-type control valve is considered in this study with dimensions similar to that recommended by Qyyum *et al.* [29]. For validation of the second model, the experimental results of Skye *et al.* [14] are used. Table 2 presents a comparison between the present geometries and the reference geometries for both models. Both RHVT models have annular-type inlet

Table 2. Comparison of geometric parameters of current models with respective reference models.

		First model		Second model
RHVT parameter	Unit	Current study	Rafiee and Sadeghiazad [8]	Current study and Skye *et al.* [14]
Working tube length (L)	mm	264	250	106
Working tube diameter (D)	mm	17.6	18	11.4
L/D	–	15	13.89	9.3
Cold outlet diameter (d_c)	mm	8.8	9	6.2
Number of nozzles	–	2	2	6

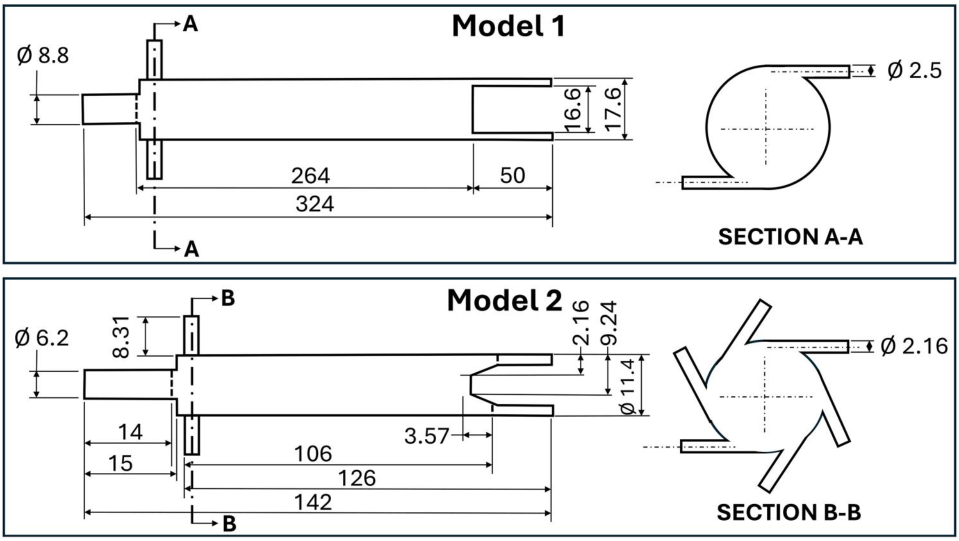

Figure 2. Dimensions of both RHVT models investigated in this study (all dimensions in mm).

tangential nozzles, as axial annular inlets have the ability to converge faster by improving numerical stability. The lengths of inlet and outlets of the flow domain were extended to account for the possible disturbances. Many studies have used this concept because it can control disturbances, and thus improving numerical stability. Figure 2 illustrates both geometric models along with their dimensions.

3.2. Evaluation parameters

The primary performance indicator of the RHVT is the temperature difference. There are three different temperature differences that can be used to assess the performance of the RHVT:

- Cold outlet temperature difference (ΔT_c): The difference between the temperature of the incoming compressed stream (T_i) and the exiting cold stream (T_c) (see Eq. 13).

$$\Delta T_c = T_i - T_c \tag{13}$$

- Total temperature difference (ΔT_t): The difference between the temperature of the hot stream (T_h) and that of the cold stream (see Eq. 14).

$$\Delta T_t = T_h - T_c \tag{14}$$

- Hot outlet temperature difference (ΔT_h): The difference between the exiting hot stream and the temperature of the incoming compressed stream (see Eq. 15).

$$\Delta T_h = T_h - T_i \tag{15}$$

In addition, the average percentage deviation of the temperature difference ($P_{\Delta T}$), is used for comparison with the experimental results. Equation (16) represents the formula to find the average percentage deviation of the temperature difference.

$$P_{\Delta T} = \left| \frac{\Delta T_{exp} - \Delta T_{cfd}}{\Delta T_{exp}} \right| \times 100\% \tag{16}$$

where ΔT_{exp} and ΔT_{cfd} are the experimental and computational temperature differences, respectively.

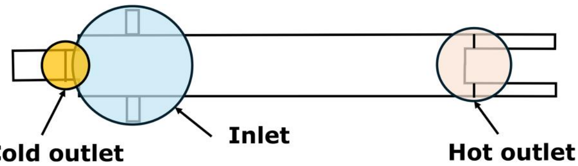

Figure 3. Regions of mesh refinement for both geometric models.

Table 3. Boundary conditions for the mesh-independence study.

Boundary	Type of boundary condition	Model 1	Model 2
Inlet	Pressure inlet	2.5 bar, 294.2 K	5.84 bar, 294.2 K
Cold outlet	Pressure outlet	1.03 bar	1.03 bar
Hot outlet	Pressure outlet	Variable to get different cold mass fraction	
Wall	Adiabatic wall with no-slip	Heat flux = 0 W/m^2	

Table 4. Final element size and number of elements for different regions of both RHVT models.

	General		Inlet		Cold outlet		Hot outlet	
Model	Size	Elements	Size	Elements	Size	Elements	Size	Elements
1	0.75	5.53	0.29	5.55	0.35	5.64	0.4	5.83
2	0.30	1.78	0.23	8.14	0.23	8.32	0.23	8.78

The unit for element size is mm and the number of elements is in millions.

3.3. Mesh-independence study

For both geometric models, a 3D CFD mesh is generated using the ANSYS Meshing tool. The mesh is composed of tetrahedral elements. The main reasons for using tetrahedral mesh elements are their geometric flexibility, conformance to boundaries, and ease of local refinement. However, it should be noted that an unstructured mesh can lead to numerical stiffness, adaptability challenges, and a larger number of elements. These challenges were overcome by refining the mesh in certain regions and by using the shared topology option available in ANSYS SpaceClaim. This is because the mesh-independence study directly affects the numerical accuracy and optimization of the computational solution. First, the general element size is refined and then the mesh is improved at the inlet and outlet regions of the RHVT until consistent results are obtained. Figure 3 shows the areas of mesh refinement for both geometric models. Mesh refinement is continued until the results no longer change. Another factor in finalizing the element size is numerical stiffness. The element size is reduced to a certain limit beyond which convergence difficulty occurs, and the results become unrealistic. Consequently, some results are not considered because their magnitudes are impractical. Furthermore, the mesh sizes that have quick convergence are preferred.

For both geometric models, static pressure and static temperature are specified as the boundary conditions at the inlets. Both the hot and cold outlets are pressure-type outlets. Adiabatic no-slip conditions are applied to the inner walls of the RHVT. The simulations are set up using ANSYS CFX. The convergence limit for the residuals is set to 10^{-6} for the mass and momentum, while the residual for heat transfer is set to 10^{-5}. Air with ideal properties is chosen as the working fluid. Steady-state simulations are performed. The boundary conditions, for both geometric models, considered for the mesh-independence study are shown in Table 3.

For the first geometric model, the SST k-ω turbulence model is employed, while for the second geometric model, the k-ϵ turbulence model is employed. Table 4 shows the final element size and the number of elements in different regions of both geometric models, whereas Figure 4 shows the final 3D mesh of both geometric models.

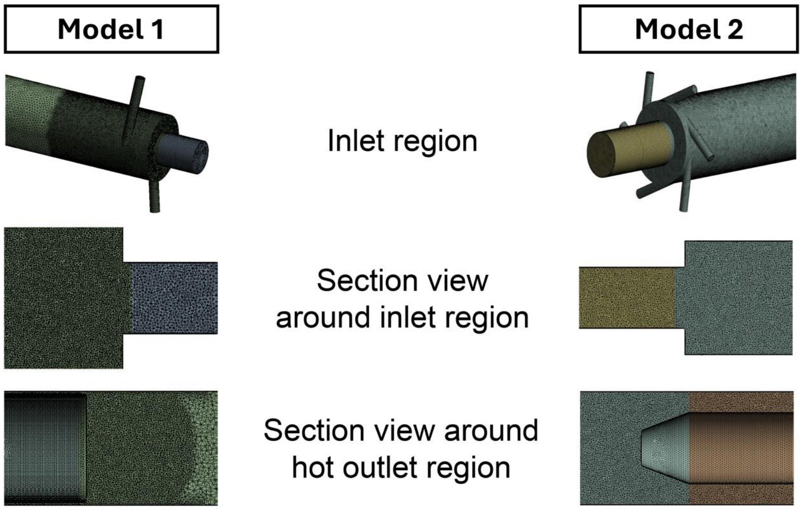

Figure 4. Final 3D mesh in different regions of both RHVT models.

Table 5. Average values of y^+ in different regions of the first RHVT model.

Region of vortex tube	Final y^+ value [–]
VT wall	1.89
VT cold outlet	1.66
VT hot outlet	1.42

3.4. y^+ study

As mentioned above, the choice of turbulence model has substantial influence on the targeted y^+ value of the RHVT. This is because the y^+ value affects the accurate capturing of the flow phenomena inside the boundary layer. y^+ is the dimensionless distance from the wall to the first cell and it indicates the quality of the mesh in the boundary layer. Inflation layers are augmented inside the RHVT to achieve the appropriate y^+ value. However, the way to ensure that correct inflation layers are included is to obtain the appropriate y^+ value. Therefore, the first layer height is adjusted to obtain different y^+ values until the solution becomes consistent and closely matches the experimental data.

For both geometric models, the first layer height is reduced until the magnitudes of temperature separation become constant. For the first geometric model, the first layer height is reduced until $y^+ < 1$ is achieved. However, below $y^+ = 2$, there is no significant improvement of results but there is numerical stiffness. Therefore, the reduction in the first layer height is stopped after achieving $y^+ < 2$. Table 5 shows the final values of y^+ in different regions of the first RHVT model.

For the second geometric model, the first layer height and number of inflation layers are varied to obtain the appropriate y^+ value. Table 6 shows the average y^+ values for different first layer heights. There is a decrease in the average y^+ value as the first layer height decreases. However, another concern is the computational effort and numerical stiffness. On the one hand, the number of mesh elements increases as the first layer height decreases, leading to an increase in computational cost. On the other hand, numerical stiffness occurs with reduction in the first layer height. The reduction in the first layer height is stopped when the results stop changing, indicating that no further improvement in results. Instead, further reduction leads to additional computational cost and numerical stiffness. Furthermore, the results are compared with the experimental data of Skye *et al.* [14]. It is noted from Table 6 that there is no significant

Table 6. Average values of y^+ for different first layer heights and number of inflation layers where the average value is the arithmetic mean of y^+ in the regions of vortex tube, cold outlet, and hot outlet.

			y^+ (–)					Current results			Experimental results*		
First layer height (mm)	Number of inflation layers	Number of elements (millions)	Vortex tube	Cold outlet	Hot outlet	Average	Cold mass fraction	ΔT_h	ΔT_c	ΔT_t	ΔT_h	ΔT_c	ΔT_t
2	13	10.47	5.99	4.50	2.54	4.34	0.58	39.63	28.72	68.34	39.20	34.08	73.28
3	12	10.17	8.98	6.77	3.85	6.53	0.57	39.23	28.59	67.82	38.48	34.80	73.28
4	11	9.91	12.03	8.97	5.21	8.74	0.56	38.36	29.07	67.43	37.49	33.98	71.47
5	10	9.69	14.41	10.85	5.69	10.32	0.63	44.64	33.64	78.28	42.16	33.23	75.39
6	10	9.60	18.12	13.35	7.92	13.13	0.55	37.59	29.54	67.13	36.21	35.36	71.57
8	10	9.43	24.43	17.54	10.79	17.59	0.53	35.57	30.86	66.43	33.52	36.21	69.73
10	10	9.27	30.90	21.25	13.41	21.85	0.50	35.43	34.11	69.54	30.97	37.49	68.46
12	10	9.09	37.52	25.63	16.40	26.52	0.49	33.37	33.24	66.61	30.12	37.91	68.03
13	10	9.01	40.94	27.59	17.88	28.80	0.48	32.25	34.08	66.33	29.73	38.05	67.78
14	10	8.93	44.25	29.61	19.05	30.97	0.47	32.09	34.33	66.42	29.98	38.34	68.32

The yellow highlighted row is selected for further analysis.
*The experimental results are obtained by linear interpolation of available data in Skye *et al*. [14].

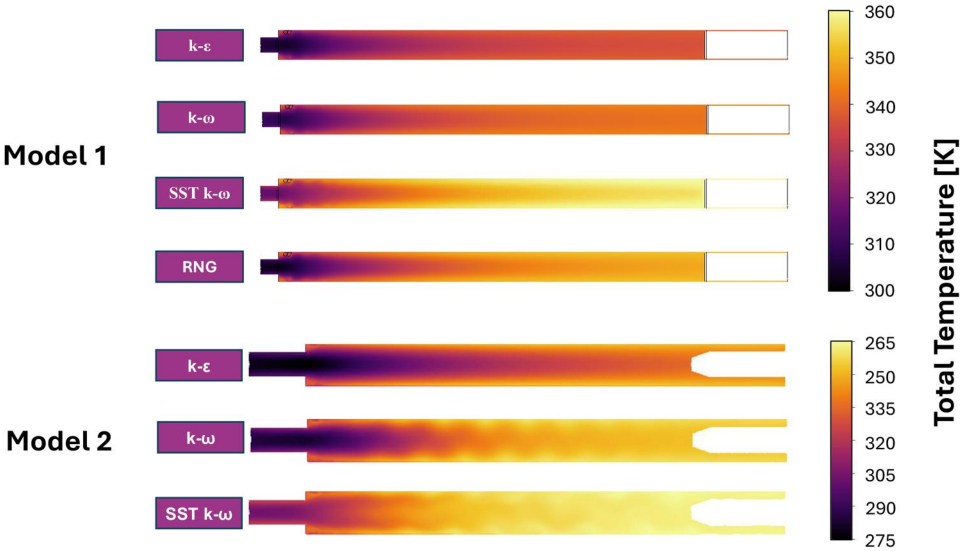

Figure 5. The local contours of total temperature obtained by different turbulence models for both geometric models.

difference between the current and the experimental results. Therefore, the first layer height of 0.002 mm with 13 inflation layers is chosen for further analysis, as going beyond this would not improve the results.

4. Results and discussion

This section discusses the results obtained from different turbulence models for both geometries. The results are validated against the respective experimental results. The comparison is mainly based on the temperature separation inside the RHVT. Qualitatively, all investigated turbulence models are able to capture the TSE. However, the choice of turbulence model has substantial influence on the magnitudes of minimum and maximum temperatures. Figure 5 compares the contours of total temperature obtained by different turbulence models for both considered RHVT geometries. It is noted here that the temperature at the core of RHVT is lower than that in the region closer to the wall of RHVT for both geometric models. For the first geometric model, the k-ϵ and k-ω turbulence models have the closest resemblance with the temperature distribution contours reported by Rafiee and Sadeghiazad [8]. However, the observation cannot be made for the second geometric model due to unavailability of the reference results.

Next, the magnitudes of temperature differences of the obtained results are compared with the reference results and Eq. (16) is used to calculate $P_{\Delta T}$. Figure 6 presents the comparison of the current results of the first geometric model with the experimental results of Rafiee and Sadeghiazad [8]. However, an important point is that Rafiee and Sadeghiazad [8] only reported the ΔT_c values; whereas, it has been reported by multiple authors that all three temperature difference values (ΔT_c, ΔT_h, and ΔT_t) should be compared to draw the final conclusion; otherwise, one could lead to conflicting opinions. Therefore, an energy balance is applied to the results of Rafiee and Sadeghiazad [8] to approximate the ΔT_h and ΔT_t values. It should be noted that perfectly adiabatic conditions are assumed by neglecting changes in potential and kinetic energy when applying the principle of energy conservation. Table 7 shows the average deviation of turbulence model results from the experimental results. From Table 7 and Figure 6, it can be concluded that the k-ϵ turbulence model has closest resemblance with the experimental results when ΔT_c, ΔT_h, and ΔT_t are considered, followed by the k-ω turbulence model. However, the

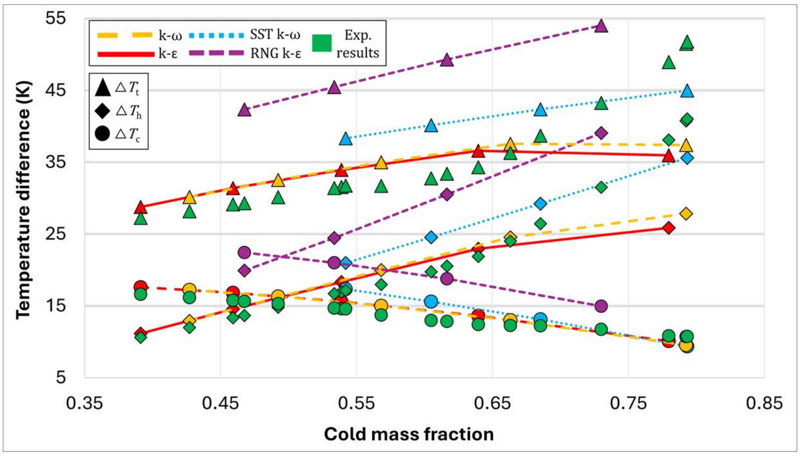

Figure 6. Comparison of temperature differences obtained by different turbulence models for the first geometric model with the experimental results of Rafiee and Sadeghiazad [8].

Table 7. $P_{\Delta T}$ obtained by different turbulence models and deviated from the experimental results of Rafiee and Sadeghiazad [8].

	Average deviation of temperature difference (%)		
Turbulence model	ΔT_h	ΔT_c	ΔT_t
k-ϵ	11.87	7.18	10.82
RNG k-ϵ	43.38	35.70	42.21
k-ω	12.47	7.87	11.25
SST k-ω	28.02	22.74	27.00

Table 8. $P_{\Delta T}$ obtained by different turbulence models and deviated from the experimental results of Skye *et al.* [14].

	Average deviation of temperature difference (%)		
Turbulence model	ΔT_h	ΔT_c	ΔT_t
k-ϵ	17.79	5.96	5.51
k-ω	20.78	3.93	10.15
SST k-ω	52.12	33.54	31.60

differences in deviation of results of k-ϵ and k-ω models from the experimental results are not very significant. Additionally, the k-ω turbulence model took longer time to converge and led to numerical stiffness. The other two turbulence models (SST k-ω and RNG k-ϵ) have significant differences in the results when compared with reference results. The present results are in line with the conclusions of most previous authors, who found that the k-ϵ turbulence model is the most suitable two-equation turbulence model for numerical analysis of RHVTs.

The results of the first RHVT model are used as a base for the second one to select the turbulence models for investigation. Three different turbulence models, namely k-ϵ, k-ω, and SST k-ω, are evaluated under the same boundary conditions. The number of readings is kept to a minimum for the k-ω and SST k-ω turbulence models to save the computational cost. Table 8 shows the average deviation of turbulence model results from the experimental results, while Figure 7 depicts the comparison of current results with experimental data. It can be seen that the k-ϵ turbulence model has the best agreement compared to other turbulence models when ΔT_c and ΔT_t are considered, while, for ΔT_h, the k-ω turbulence model has the closest agreement with the experimental results. However, again the k-ω model results in numerical stiffness and increase in computational cost. Therefore, based on the overall results, it can be concluded that k-ϵ is the most appropriate turbulence model for numerical analysis of the RHVTs.

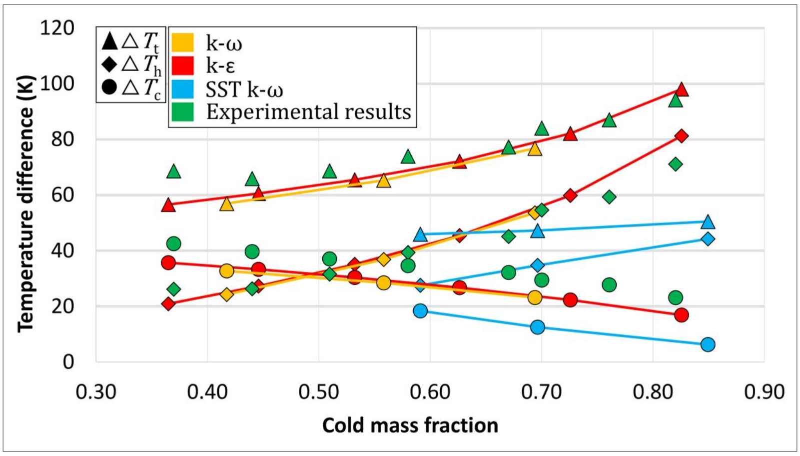

Figure 7. Comparison of temperature difference obtained by different turbulence models for the first model with the experimental results of Skye *et al.* [14].

The present results show that although the SST k-ω turbulence model is a combination of the k-ϵ and k-ω turbulence models, its performance is significantly worse than that of these individual models. Moreover, while two-equation RANS turbulence models provide advantages, such as faster convergence and lower computational cost for approximating flow inside the RHVT, advance techniques like DNS, LES, and RSM can be utilized to further increase accuracy and reveal critical intricacies. However, these advanced techniques are associated with more complex numerical setups and increased computational costs.

5. Conclusions and future work

In this study, a 3D numerical analysis of two different RHVT models have been performed to find the most suitable two-equation RANS turbulence model for use. For the first geometric model, four different turbulence models are considered: k-ϵ, k-ω, SST k-ω, and RNG k-ϵ. For the second geometric model, three different turbulence models are evaluated: k-ϵ, k-ω, and SST k-ω. Furthermore, different turbulence models are used for the mesh-independence study for each geometric model: for the first one, SST k-ω of low-Re number type is used and for the second one, k-ϵ of high-Re number type is used. Based on the outcomes of this numerical study, following conclusions can be drawn:

- Qualitatively all models are able to capture the TSE for both geometric models. However, the magnitudes of maximum and minimum temperature are significantly influenced by the choice of turbulence model. No turbulence model is able to predict the exact temperature magnitudes when compared to the reference data.
- Quantitively, for both geometric models, the k-ϵ and k-ω have the closest agreement with the respective experimental data. However, k-ω has numerical stiffness and it takes longer time to converge than k-ϵ. Additionally, the obtained results for the k-ϵ turbulence model are almost consistent with the conclusions of previous studies.
- Based on the results, the k-ϵ turbulence model appears to be the most appropriate two-equation RANS turbulence model for analysis of RHVTs. Therefore, it is recommended to use it for further numerical studies.

Furthermore, a recirculation zone is identified between the cold and hot flows inside the RHVT. This could be further refined in the future for more accurate results using two-equation

RANS turbulence models. In addition to that, it is important to know that although a good prediction of the actual flow can be obtained by two-equation turbulence models, LES and RSM can produce even more accurate results. Nevertheless, LES and RSM demand higher computational cost. That is why two-equation turbulence models are preferred. Although some authors have reported in the past that RSM leads to numerical divergence [14,19], some reported it be more accurate than two-equation RANS turbulence models [8,30]. Therefore, it is necessary to test whether LES or RSM calculations provide the same level of accuracy for TSE results as two-equation RANS turbulence models, and whether the flow field properties behave similarly. If they do, then the k-ϵ model can serve as a quick and approximate performance estimation tool. Otherwise, the k-ϵ model may not be suitable as a convenient tool to unravel the complexities of RHVTs, and advanced techniques should then be used.

Disclosure statement

No potential conflict of interest was reported by the author(s).

ORCID

O. A. A. Awan http://orcid.org/0000-0001-7735-8631
R. Sager http://orcid.org/0009-0002-5762-1257
E. Juntasaro http://orcid.org/0000-0001-7986-5856

References

[1] R. Hilsch, "The use of the expansion of gases in a centrifugal field as cooling process," *Rev. Sci. Instrum.*, vol. 18, no. 2, pp. 108–113, Feb. 1947. DOI: 10.1063/1.1740893.

[2] B. K. Ahlborn and J. M. Gordon, "The vortex tube as a classic thermodynamic refrigeration cycle," *J. Appl. Phys.*, vol. 88, no. 6, pp. 3645–3653, Sep. 2000. DOI: 10.1063/1.1289524.

[3] T. H. Cetin and J. Zhu, "Thermodynamic assessment of a novel self-condensing sCO_2 recompression system with vortex tube," *Energy Convers. Manag.*, vol. 269, pp. 116110, 2022. DOI: 10.1016/j.enconman.2022.116110.

[4] A. Mansour, R. Oberti, H. Nesreddine, and S. Poncet, "Thermodynamic analysis of a transcritical CO_2 heat pump integrating a vortex tube," *Appl. Therm. Eng.*, vol. 224, pp. 120076, Apr. 2023. DOI: 10.1016/j.applthermaleng.2023.120076.

[5] A. Aghagoli, M. Sorin, and S. Poncet, "Thermodynamics analysis of a novel transcritical CO_2 vortex tube heat pump cycle," Proceedings of 27th CANCAM, vol. 4, May. 2019.

[6] M. Baghdad, A. Ouadha, O. Imine, and Y. Addad, "Numerical study of energy separation in a vortex tube with different RANS models," *Int. J. Therm. Sci.*, vol. 50, no. 12, pp. 2377–2385, Dec. 2011. DOI: 10.1016/j.ijthermalsci.2011.07.011.

[7] V. Bianco, A. Khait, A. Noskov, and V. Alekhin, "A comparison of the application of RSM and LES turbulence models in the numerical simulation of thermal and flow patterns in a double-circuit Ranque-Hilsch vortex tube," *Appl. Therm. Eng.*, vol. 106, pp. 1244–1256, Aug. 2016. DOI: 10.1016/j.applthermaleng.2016.06.095.

[8] S. E. Rafiee, S. Ayenehpour, and M. M. Sadeghiazad, "A study on the optimization of the angle of curvature for a Ranque–Hilsch vortex tube, using both experimental and full Reynolds stress turbulence numerical modelling," *Heat Mass Transf.*, vol. 52, no. 2, pp. 337–350, Apr. 2016. DOI: 10.1007/s00231-015-1562-y.

[9] T. K. Sharma, G. A. Rao, and K. M. Murthy, "Numerical analysis of a vortex tube: a review," *Arch. Comput. Methods Eng.*, vol. 24, pp. 251–280, Jan. 2017. DOI: 10.1007/s11831-016-9166-3.

[10] A. Bazgir, M. R. Khosravi-Nikou, and A. Heydari, "Numerical CFD analysis and experimental investigation of the geometric performance parameter influences on the counter-flow Ranque-Hilsch vortex tube (C-RHVT) by using optimized turbulence model," *Heat Mass Transf.*, vol. 55, no. 9, pp. 2559–2591, Mar. 2019. DOI: 10.1007/s00231-019-02578-1.

[11] R. Chýlek, L. Šnajdárek, and J. Pospíšil, "Vortex tube: a comparison of experimental and CFD analysis featuring different RANS models," *MATEC Web Conf.*, vol. 168, pp. 02012, 2018. DOI: 10.1051/matecconf/201816802012.

[12] A. Secchiaroli, R. Ricci, S. Montelpare, and V. D'alessandro, "Numerical simulation of turbulent flow in a Ranque–Hilsch vortex tube," *Int. J. Heat Mass Transf.*, vol. 52, no. 23–24, pp. 5496–5511, Nov. 2009. DOI: 10.1016/j.ijheatmasstransfer.2009.05.031.

[13] H. Khazaei, A. R. Teymourtash, and M. Malek-Jafarian, "Effects of gas properties and geometrical parameters on performance of a vortex tube," *Sci. Iran.*, vol. 19, no. 3, pp. 454–462, Jun. 2012. DOI: 10.1016/j.scient.2012.03.003.

[14] H. M. Skye, G. F. Nellis, and S. A. Klein, "Comparison of CFD analysis to empirical data in a commercial vortex tube," *Int. J. Refrigeration*, vol. 29, no. 1, pp. 71–80, Jan. 2006. DOI: 10.1016/j.ijrefrig.2005.05.004.

[15] X. Guo, B. Zhang, and Y. Shan, "LES study on the working mechanism of large-scale precessing vortices and energy separation process of Ranque-Hilsch vortex tube," *Int. J. Therm. Sci.*, vol. 163, pp. 106818, May 2021. DOI: 10.1016/j.ijthermalsci.2020.106818.

[16] T. Farouk and B. Farouk, "Large eddy simulations of the flow field and temperature separation in the Ranque-Hilsch vortex tube," *Int. J. Heat Mass Transf.*, vol. 50, no. 23–24, pp. 4724–4735, Nov. 2007. DOI: 10.1016/j.ijheatmasstransfer.2007.03.048.

[17] R. K. Singh, A. K. Pramanick, and S. C. Rana, "Computational study of temperature separation for a three-dimensional vortex tube with cold exit diameter and nozzle number variation," *Int. J. Ambient Energy*, vol. 43, no. 1, pp. 7046–7060, Apr. 2022. DOI: 10.1080/01430750.2022.2059001.

[18] N. J. Dyck, M. J. Parker, and A. G. Straatman, "The impact of boundary treatment and turbulence model on CFD simulations of the Ranque-Hilsch vortex tube," *Int. J. Refrigeration*, vol. 141, pp. 158–172, Sep. 2022. DOI: 10.1016/j.ijrefrig.2022.05.016.

[19] J. Lagrandeur, S. Croquer, S. Poncet, and M. Sorin, "A 2D numerical benchmark of an air Ranque-Hilsch vortex tube based on a fractional factorial design," *Int. Commun. Heat Mass Transf.*, vol. 125, pp. 105310, Jun. 2021. DOI: 10.1016/j.icheatmasstransfer.2021.105310.

[20] J. Sadeghiseraji, J. Moradicheghamahi, and A. Sedaghatkish, "Investigation of a vortex tube using three different RANS-based turbulence models," *J. Therm. Anal. Calorim.*, vol. 143, no. 6, pp. 4039–4056, Feb. 2021. DOI: 10.1007/s10973-020-09368-6.

[21] Z. Hu, R. Li, X. Yang, M. Yang, R. Day, and H. Wu, "Energy separation for Ranque-Hilsch vortex tube: a short review," *Therm. Sci. Eng. Prog.*, vol. 19, pp. 100559, Oct. 2020. DOI: 10.1016/j.tsep.2020.100559.

[22] H. R. Thakare and A. D. Parekh, "CFD analysis of energy separation of vortex tube employing different gases, turbulence models and discretisation schemes," *Int. J. Heat Mass Transf.*, vol. 78, pp. 360–370, Nov. 2014. DOI: 10.1016/j.ijheatmasstransfer.2014.06.083.

[23] X. Liu and Z. Liu, "Investigation of the energy separation effect and flow mechanism inside a vortex tube," *Appl. Therm. Eng.*, vol. 67, no. 1–2, pp. 494–506, Jun. 2014. DOI: 10.1016/j.applthermaleng.2014.03.071.

[24] S. Eiamsa-Ard and P. Promvonge, "Numerical simulation of flow field and temperature separation in a vortex tube," *Int. Commun. Heat Mass Transf.*, vol. 35, no. 8, pp. 937–947, Oct. 2008. DOI: 10.1016/j.icheatmasstransfer.2008.04.010.

[25] S. E. Rafiee and M. M. Sadeghiazad, "Three-dimensional and experimental investigation on the effect of cone length of throttle valve on thermal performance of a vortex tube using k-ϵ turbulence model," *Appl. Therm. Eng.*, vol. 66, no. 1–2, pp. 65–74, May 2014. DOI: 10.1016/j.applthermaleng.2014.01.073.

[26] F. M. White, C. O. Ng, and S. Saimek, *Fluid Mechanics*, 7th ed. New York, NY: McGraw-Hill, 2011.

[27] P. A. Durbin and B. Pettersson-Reif, *Statistical Theory and Modeling for Turbulent Flows*, 2nd ed. Chichester: John Wiley and Sons, 2011.

[28] Exair, "Model 3225 Vortex Tube," Exair. https://www.exair.com/3225.html. Accessed: May 30, 2024.

[29] M. A. Qyyum, A. A. Noon, F. Wei, and M. Lee, "Vortex tube shape optimization for hot control valves through computational fluid dynamics," *Int. J. Refrigeration*, vol. 102, pp. 151–158, Jun. 2019. DOI: 10.1016/j.ijrefrig.2019.02.014.

[30] G. Suresh Kumar, B. Veerabhadra Reddy, G. Sankaraiah, and P. Venkateshwar Reddy, "Modeling the performance of vortex tube using response surface methodology and artificial neural networks," *IOP Conf. Ser. Mater. Sci. Eng.*, vol. 390, pp. 012010, 2018. DOI: 10.1088/1757-899X/390/1/012010.